Supporting Information

"All-organic" Electrode Material Toward High-Performing Rigid to Flexible Supercapacitor Devices

Pradeep Sachan, Priyanka Makkar, Ankur Malik, and Prakash Chandra Mondal*

Department of Chemistry, Indian Institute of Technology Kanpur, Uttar Pradesh-208016, India

E-mail: pcmondal@iitk.ac.in (PCM)

Contents

1) Characterization of PDI-AB molecule……...…..…….…...S3

1.1) NMR spectrum……...……. S3

1.2) Mass spectrum…….…....S4

2) TGA spectrum…….…...S4

3) FT-IR spectra……..…….……..…S5

4) UV-Vis spectrum of PDI and PDI-AB……..……S5

5) Cyclic voltammogram of PDI and PDI-AB ……..…….……..S6

6) Preparation of PDI-AB/ITO film through drop-casting…….…S6

7) UV-Vis spectrum of PDI-AB in solution and film……...…S6

8) Optical microscopy for morphology and thickness measurement.....S7

9) Density functional theory (DFT) study…….……..……..S8

10) Determination of HOMO and LUMO for PDI-AB molecule……..……....S9

11) GCD data at various mass loading of PDI-AB molecule on ITO electrode…….……..…...S9

12) Electrochemical performance of SSC devices……..…..…...S10

13) Peak current of PDI-AB molecule for first and second redox peak……..……S10

14) Cyclic stability of ITO/PDI-AB//PMMA-LiClO$_4$-PC//PDI-AB/ITO device with rigid ITO electrode……..……..…....S11

15) NMR spectrum of PDI-AB after 2000th GCD cycles ….…….…….……S12

16) Mass data of PDI-AB after 2000th GCD cycles …….……S12

17) X-ray photoelectron spectra of PDI-AB after 2000th GCD cycles ……..S13

18) FE-SEM image of PDI-AB before and after 2000th GCD cycles.…….,…….....S13

19) Log j vs. Log ν (b-value) plots…….……..……..…S14

20) j (V).$\nu^{-1/2}$ vs. $\nu^{1/2}$ plot …….…….…….....S15

21) Electrochemical impedance spectra for SSC device ……S15

22) Cyclic stability and different bend angles measurement ….……....S16

23) Electrochemical parameters for equivalent circuit model.....……..S17

24) Photocurrent measurements ….…….……..…….....S18

25) References…….....S19

1) Characterization of PDI-AB molecule:

1.1) ^{1}H and $^{13}C\{^{1}H\}$ NMR spectrum:

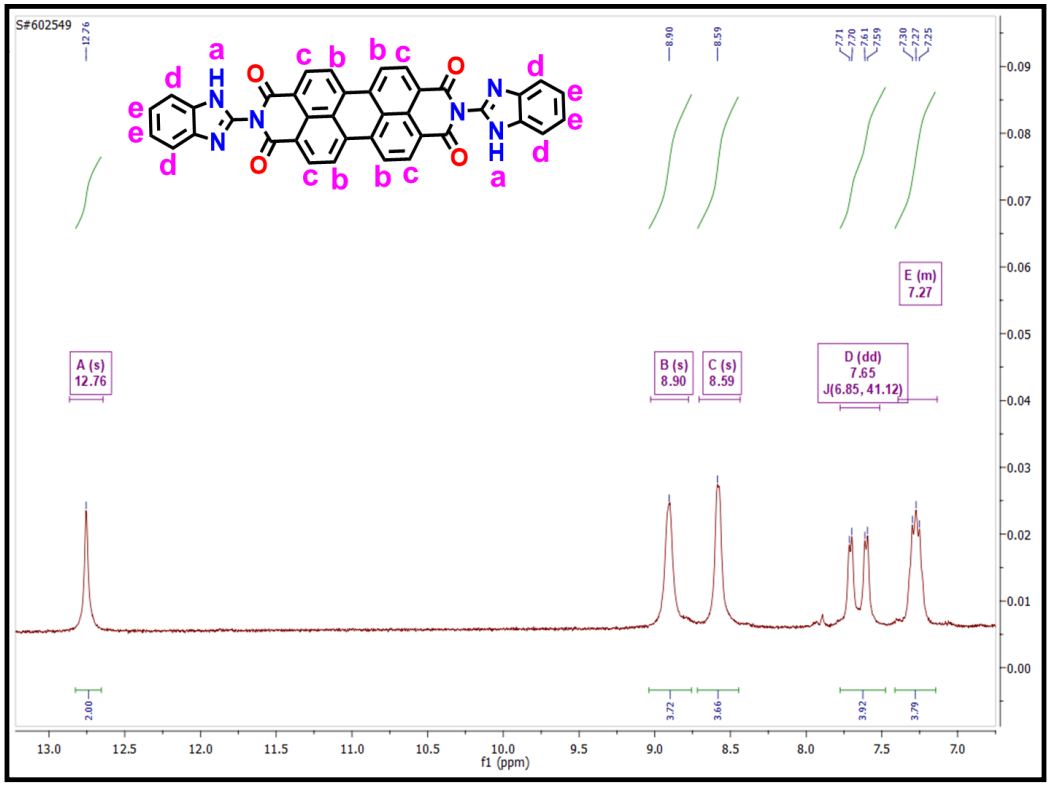

Figure S1: ^{1}H NMR spectrum of PDI-AB recorded in DMSO-d_6. Peak positions in the spectrum were assigned relative to the TMS reference, and integration was conducted by treating the NH peak as equivalent to one hydrogen atom.

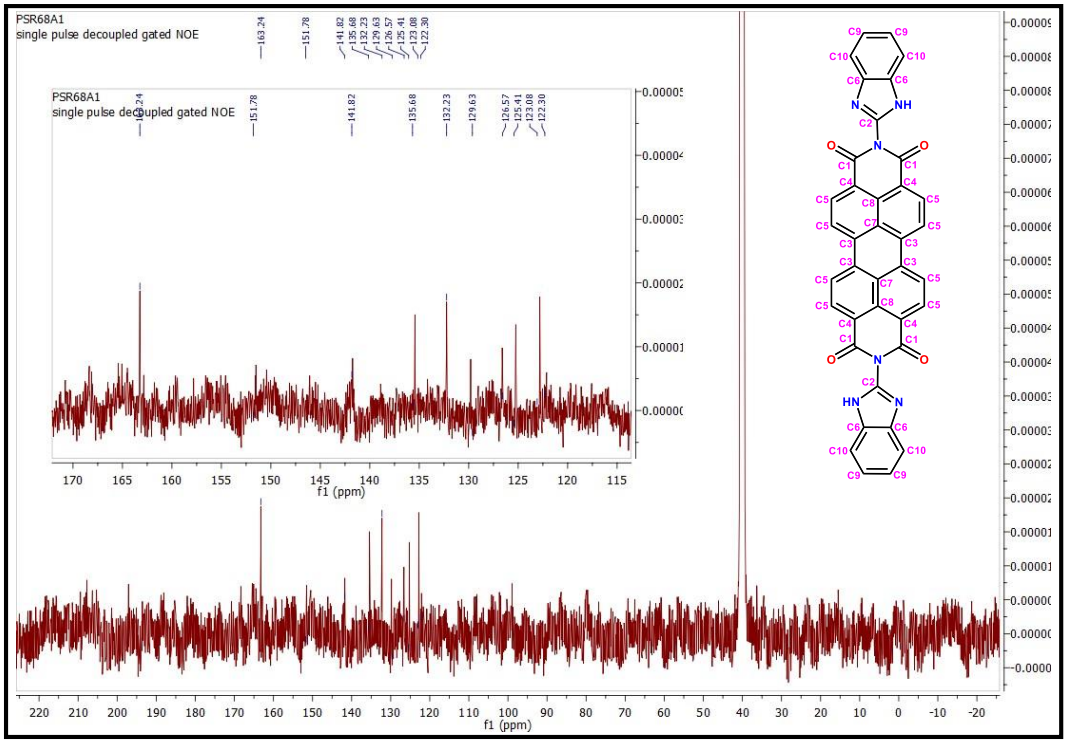

Figure S2: $^{13}C\{^{1}H\}$ NMR spectrum of PDI-AB recorded in DMSO-d_6**.** Peak positions in the spectrum were assigned relative to the TMS reference.

1.2) Mass spectrum:

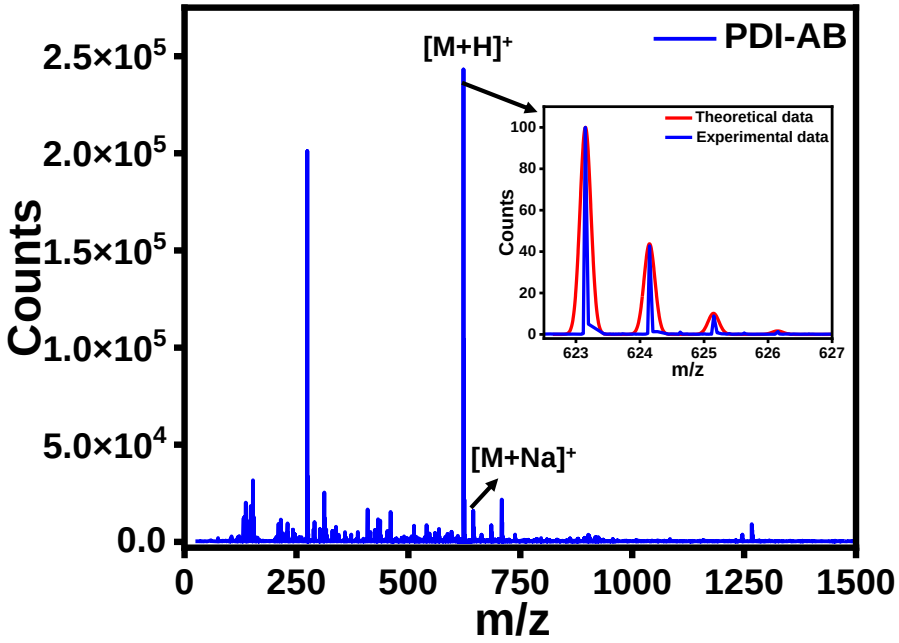

Figure S3: HRMS (ESI-MS, positive mode) of PDI-AB mass spectrum. The full-scan mass spectra revealed an isotope pattern match at 623.96 (m/z), as displayed in the zoomed image with intensity ratio (1:0.4:0.1:0.05).

2. TGA spectrum:

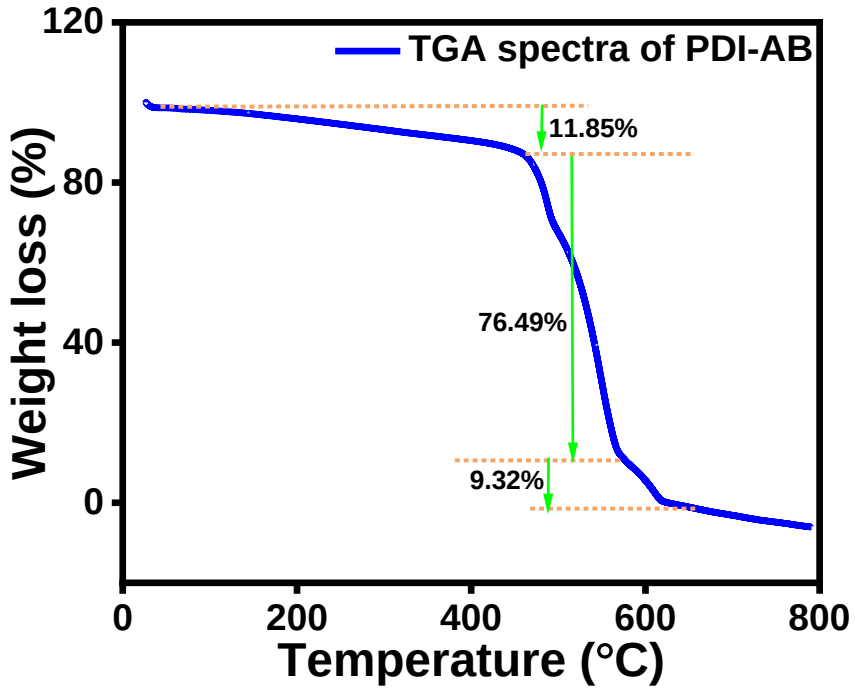

Figure S4: TGA spectrum of PDI-AB molecule in terms of % of weight loss by increasing temperature.

3. FT-IR spectra:

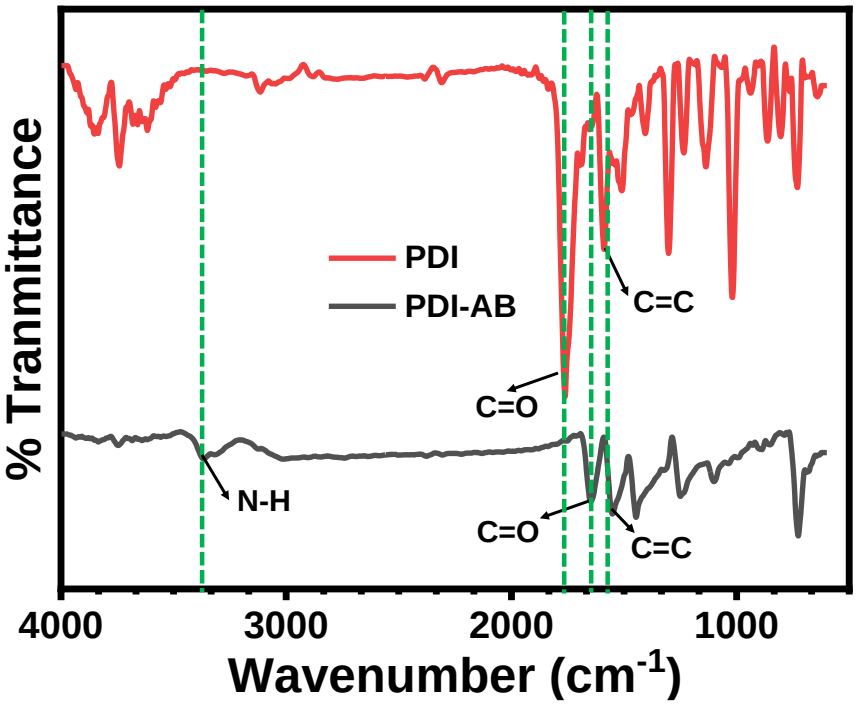

Figure S5: Comparison of FT-IR spectrum of PDI molecule (Red) and PDI-AB molecule (Black). The characteristic stretching frequencies are highlighted.

4. UV-Vis spectrum of PDI and PDI-AB:

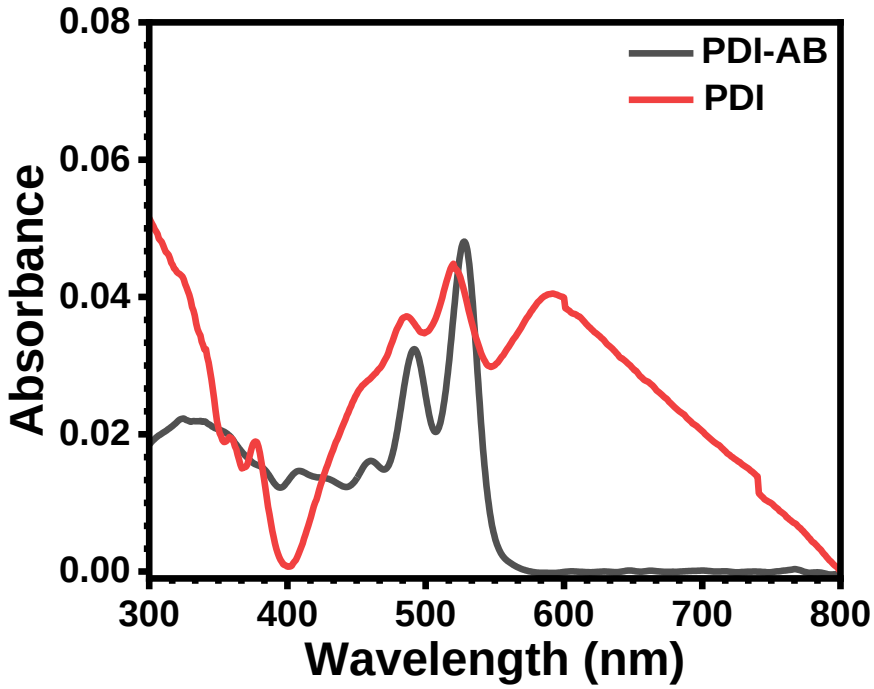

Figure S6: Comparison of UV-Vis spectrum of PDI-AB (black), and PDI (red) recorded in diluted solution (DMF as solvent).

5. **Cyclic voltammogram of PDI and PDI-AB:**

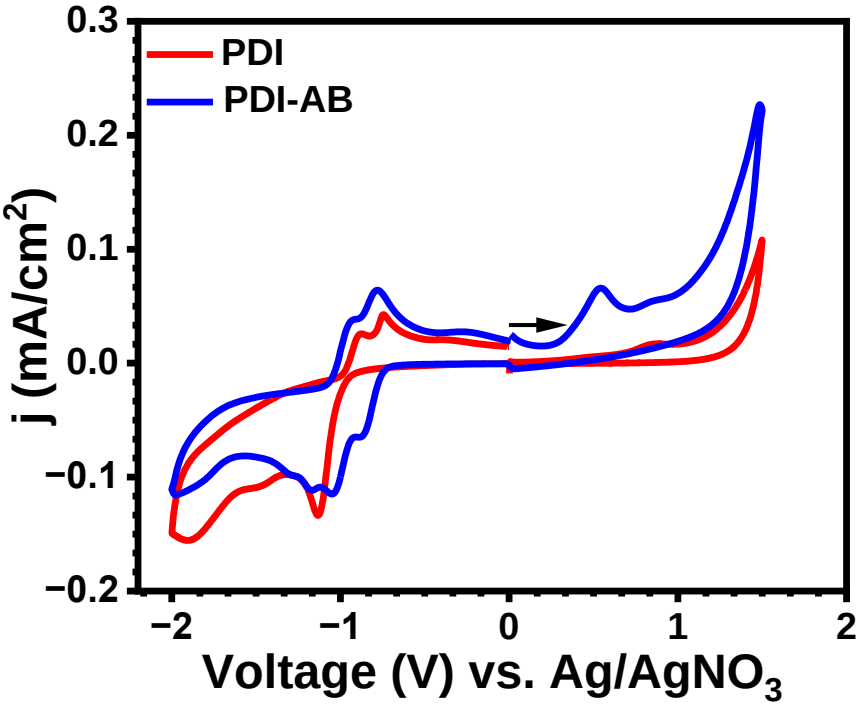

Figure S7: Cyclic voltammograms of PDI and PDI-AB, where ITO, $Ag/AgNO_3$, and a Pt wire as a working, reference, and counter electrodes, respectively. The CV was recorded at a scan rate of 100 mV/s.

6. **Preparation of PDI-AB/ITO film through drop-casting:**

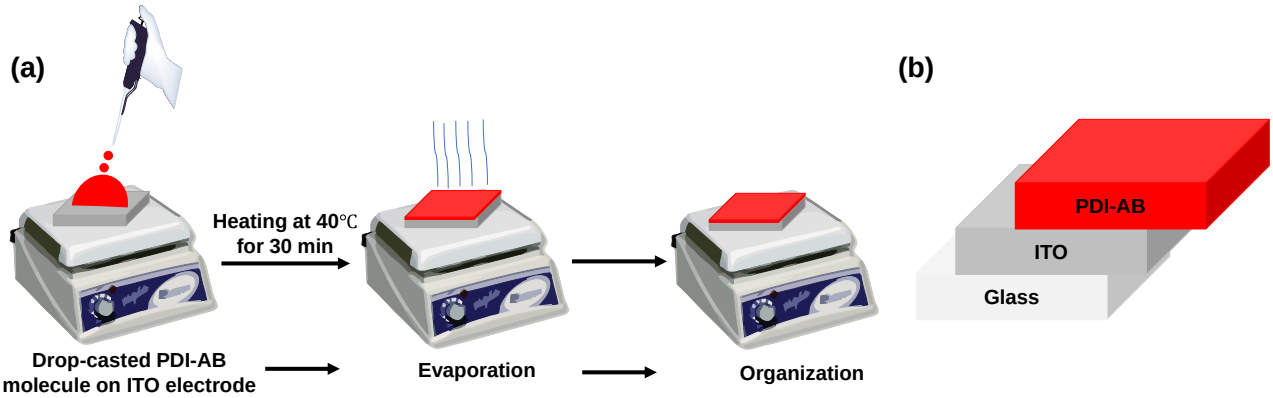

Figure S8: Stepwise representation to prepare PDI-AB/ITO electrode made via drop-casting method.

7. **UV-Vis spectrum of PDI-AB in solution and film:** The UV-Vis spectrum of PDI-AB was recorded in DMF solvent and PDI-AB/ITO. The absorption spectrum of thin films displays broad and blue-shifted **(Figure S9)**.

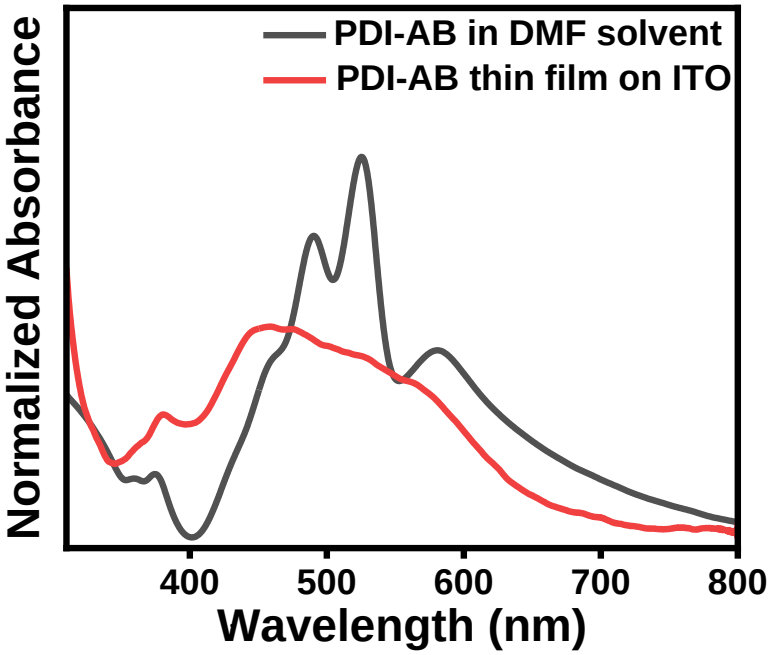

Figure S9: Comparison of UV-Vis absorption spectrum of PDI-AB in DMF solution (Black) and thin film on ITO electrode (Red).

8. Optical microscopy for morphology and thickness measurement:

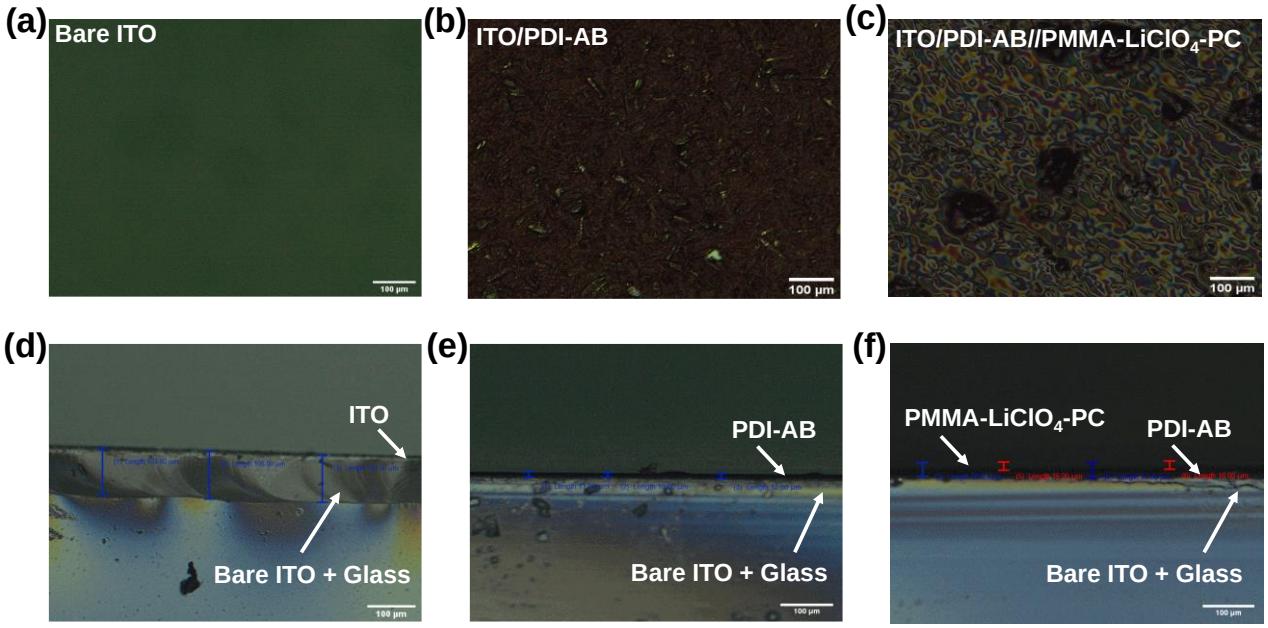

Figure S10: Morphology and cross-sectional images to deduce the material morphology and thickness of drop-casted PDI-AB and PDI-AB//PMMA-LiClO$_4$-PC as compared to bare ITO.

Table S1: The average thicknesses of the respective layers are provided in the table.

S. No.	Material	Thickness (T_1, μm)	Thickness (T_2, μm)	Thickness (T_3, μm)	Average thickness (T_A, μm)
1.	PDI-AB	11	10	12	10.15 ± 0.63
2.	PMMA-LiClO$_4$-PC	15	16	16	15.66 ± 0.57

9. **Density functional theory (DFT) study:** DFT calculated were performed to optimize the model structures and to predict the energy levels frontier orbitals of PDI and PDI-AB molecule by using B3LYP functional and 6-31+G(d,p) basis set, as implemented in the Gaussian 09 program.[1] Graphical output files were generated with the help of the GaussView program (version 6.0) **(Figure S11)**. Furthermore, we investigated the Highest Occupied Molecular Orbital (HOMO) and Lowest Unoccupied Molecular Orbital (LUMO) energies, band gap (Eg), electron affinity (EA), and ionization potential (IP) of both PDI and PDI-AB molecules. In addition to modifying the HOMO-LUMO levels of the molecule, the introduction of substituents (2-Aminobenzimidazole) to imide position induces a twist in the perylene ring. To mitigate electrostatic repulsions between the substituents and hydrogen atoms on opposite bay positions, the perylene ring stabilizes into a twisted geometry. A schematic representation of the dihedral angles formed between 2-Aminobenzimidazole and perylene rings is presented in the main text **Figure 1c**, illustrating angles of θ_1 (88.19°) and θ_2 (91.73°). Changes in these dihedral angles in a neutral PDI derivative can influence the relative energies of its reduced forms, such as the radical anion and dianion.

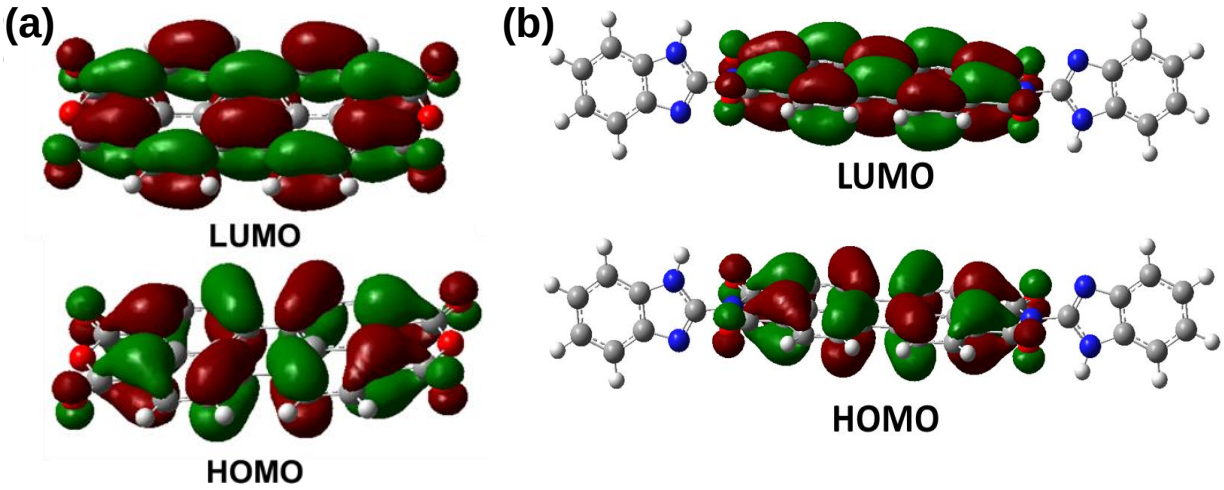

Figure S11: HOMO and LUMO contours of (a) PDI molecule, and (b) PDI-AB molecule.

10. Determination of HOMO and LUMO for PDI-AB molecule:

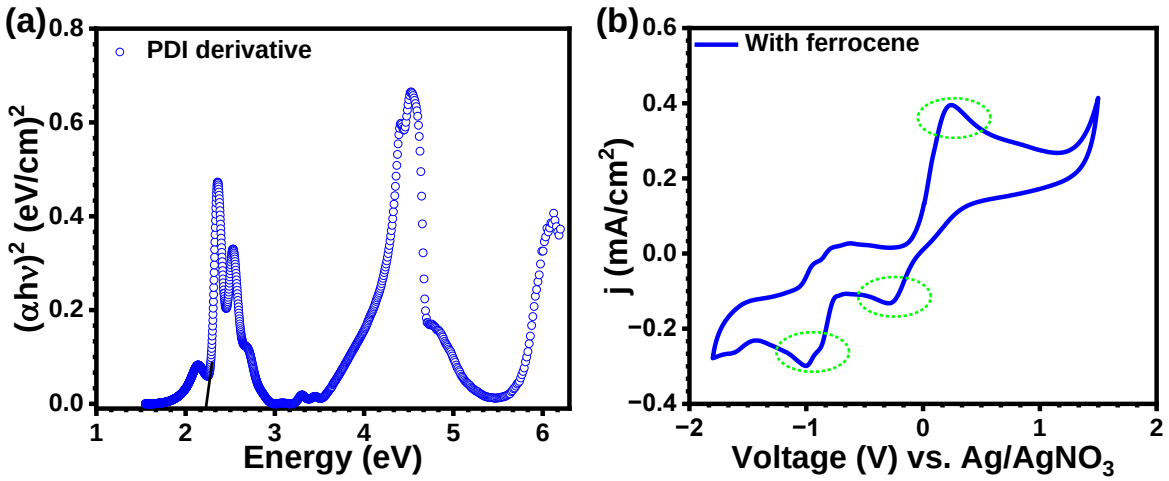

Figure S12: (a) Tauc plot of PDI-AB in dimethylformamide solution, and (b) CVs of PDI-AB in dimethylformamide solution with the presence of ferrocene, where ITO, $Ag/AgNO_3$, and a Pt wire as a working, reference, and counter electrodes, respectively. The CV was recorded at a scan rate of 50 mV/s.

11. GCD data at various mass loading of PDI-AB molecule on ITO electrode:

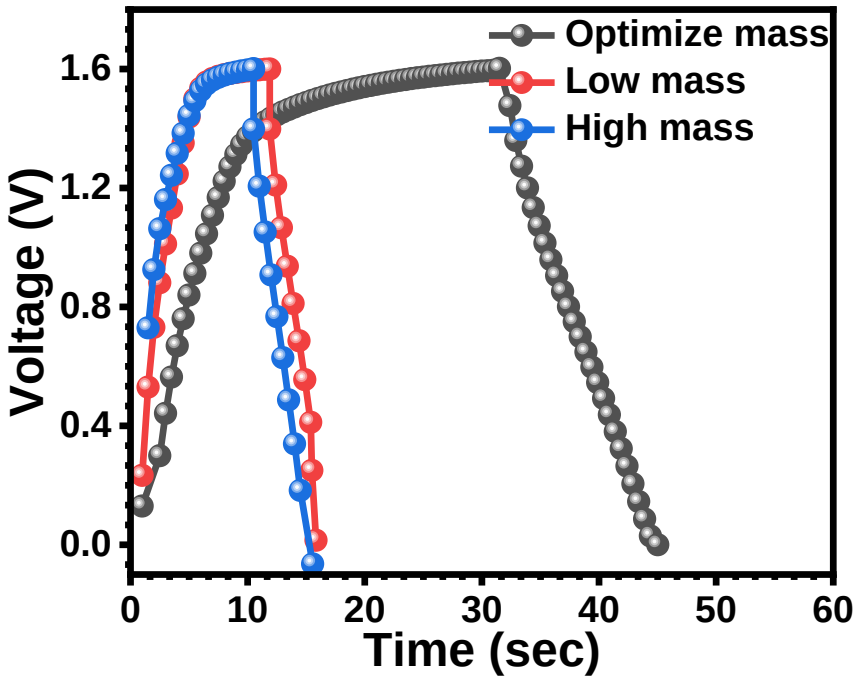

Figure S13: GCD curves of ITO/PDI-AB//PMMA-$LiClO_4$-PC//PDI-AB/ITO device at a current density of 1 mA/g with various mass loading.

Table S2: Specific capacitance (C_S) values with varying mass loading			
S. No.	**Material**	**Mass loading**	**Specific capacitance (C_S) (mF/g)**
1.	ITO/PDI-AB//PMMA-$LiClO_4$-PC//PDI-AB/ITO	1 mg	12.83±1.11
2.	ITO/PDI-AB//PMMA-$LiClO_4$-PC//PDI-AB/ITO	2 mg	33.25±0.45
3.	ITO/PDI-AB//PMMA-$LiClO_4$-PC//PDI-AB/ITO	3 mg	12.87±0.36

12. Electrochemical performance of SSC devices:

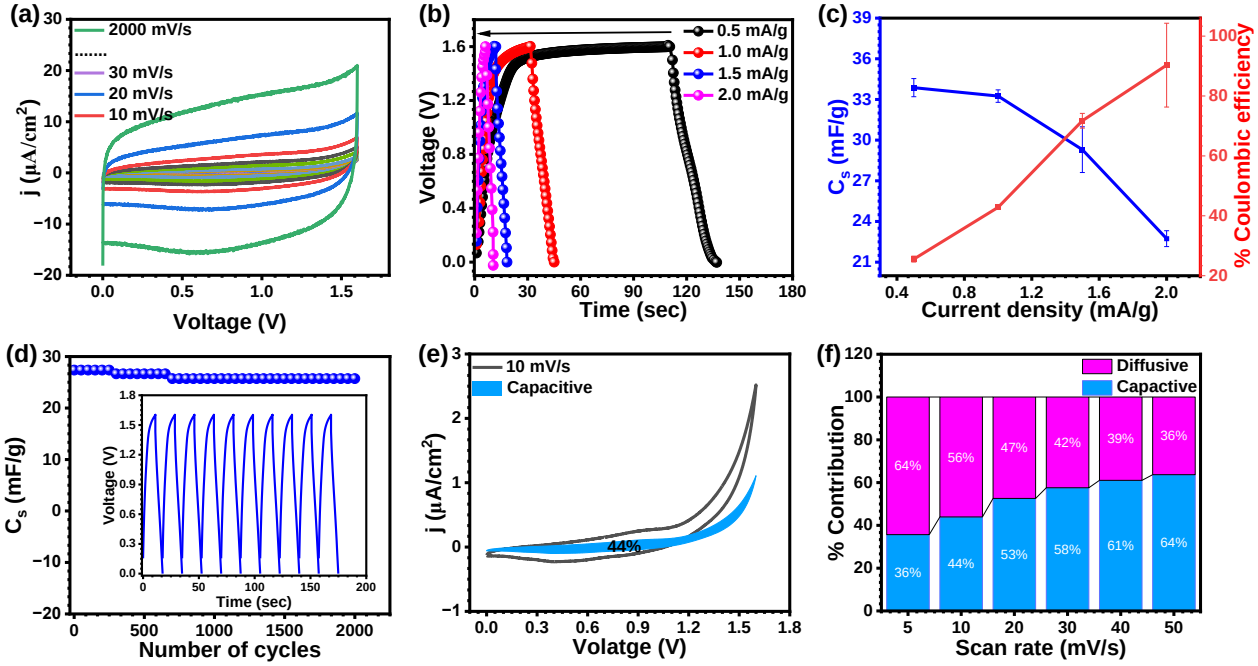

Figure S14: (a) Cyclic voltammogram at varying scan rates (5-2000 mV/s), (b) GCD curves at varying current density, (c) Variation of current density vs. C_S and columbic efficiency, (d) GCD cycle stability up to 2000 cycles at 1.5 mA/g, (e) CV at 10 mV/s showing capacitive (blue) and diffusion-controlled (white) charge storage process, and (f) Diffusion controlled and non-diffusion-controlled contribution to total C_S at various scan rates for rigid ITO/PDI-AB//PMMA-$LiClO_4$-PC//PDI-AB/ITO SSC device.

13. Peak current of PDI-AB molecule for first and second redox peak:

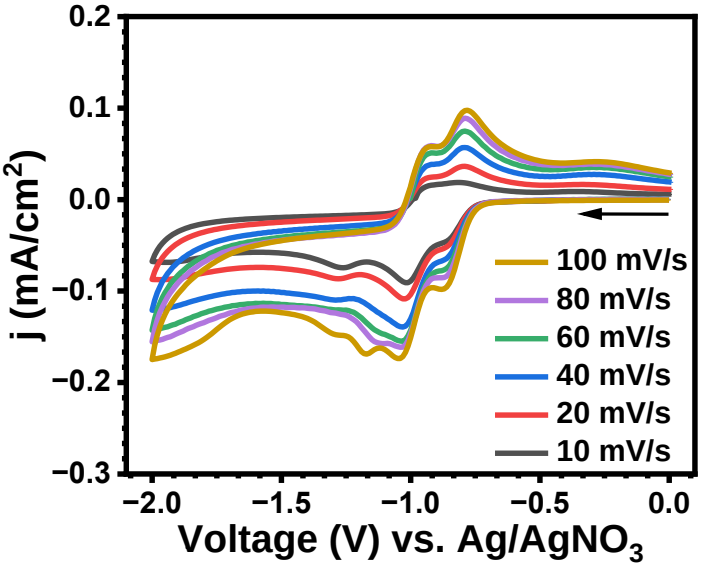

Figure S15: Cyclic voltammograms of PDI-AB (1 mM) and $LiClO_4$ as a supporting electrolyte (3 mM) recorded in dimethylformamide at different scan rates, where ITO as a working electrode, Pt wire as a counter electrode, and $Ag/AgNO_3$ as a reference electrode.

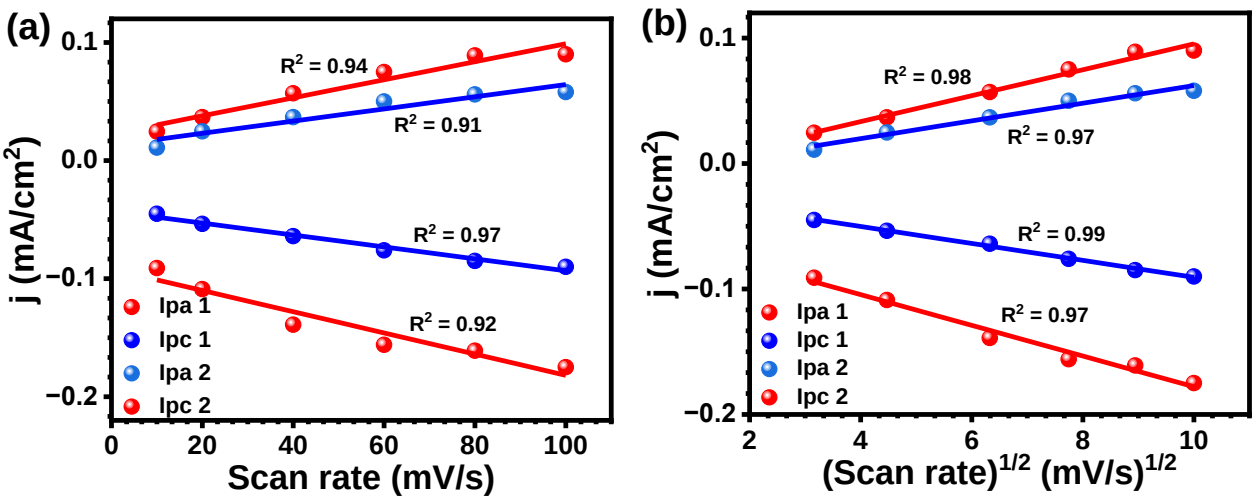

Figure S16: The relationship between peak current with (a) scan rate, and (b) square root of scan rate.

14. Cyclic stability of ITO/PDI-AB//PMMA-LiClO$_4$-PC//PDI-AB/ITO device with rigid ITO electrode:

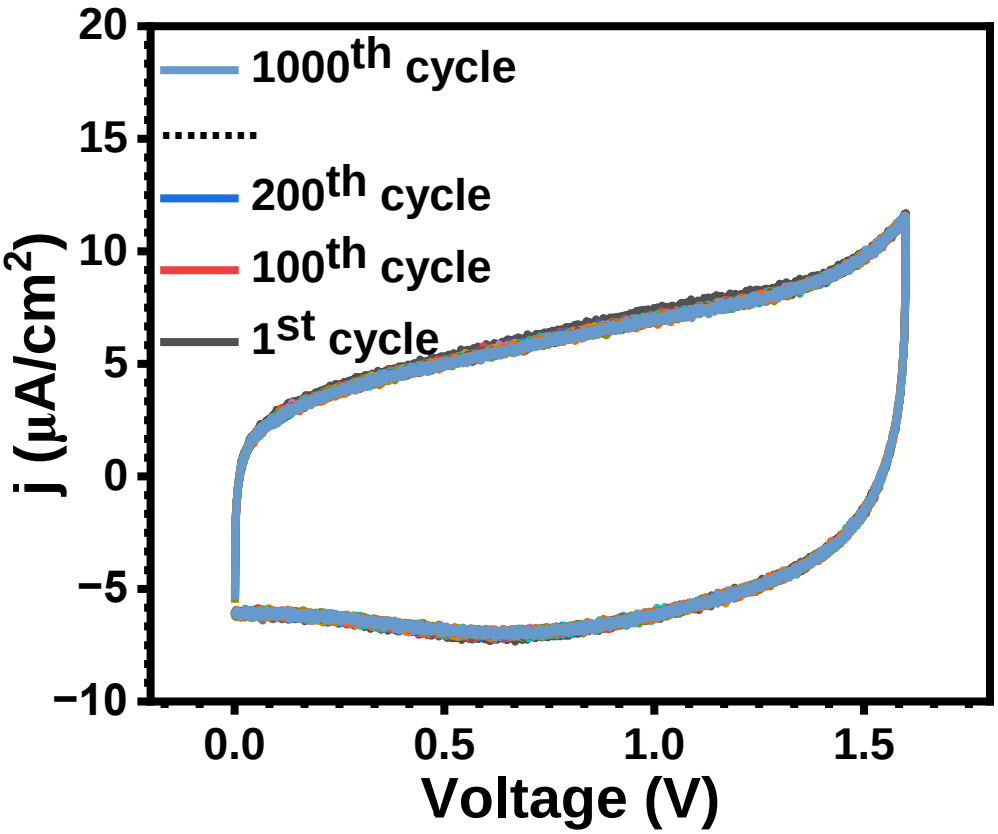

Figure S17: JV hysteresis loop of ITO/PDI-AB//PMMA-LiClO$_4$-PC//PDI-AB/ITO device with 0 to +1.6 V potential window at 1000 mV/s scan rates up to 1000 cycles.

15. NMR spectrum of PDI-AB after 2000th GCD cycles: The ^{1}H NMR spectrum of the PDI-AB molecule was recorded in DMSO-d_6 after completing 2000th GCD cycles at a current density of 1.5 mA/g to assess the stability of the organic material. This spectrum was compared with a previous ^{1}H NMR spectrum of the same molecule. The ^{1}H NMR spectrum of PDI-AB (green) after GCD cycling includes additional peaks in the non-aromatic region, which are attributed to the presence of PMMA-$LiClO_4$-PC and Nafion in the PDI-AB sample.

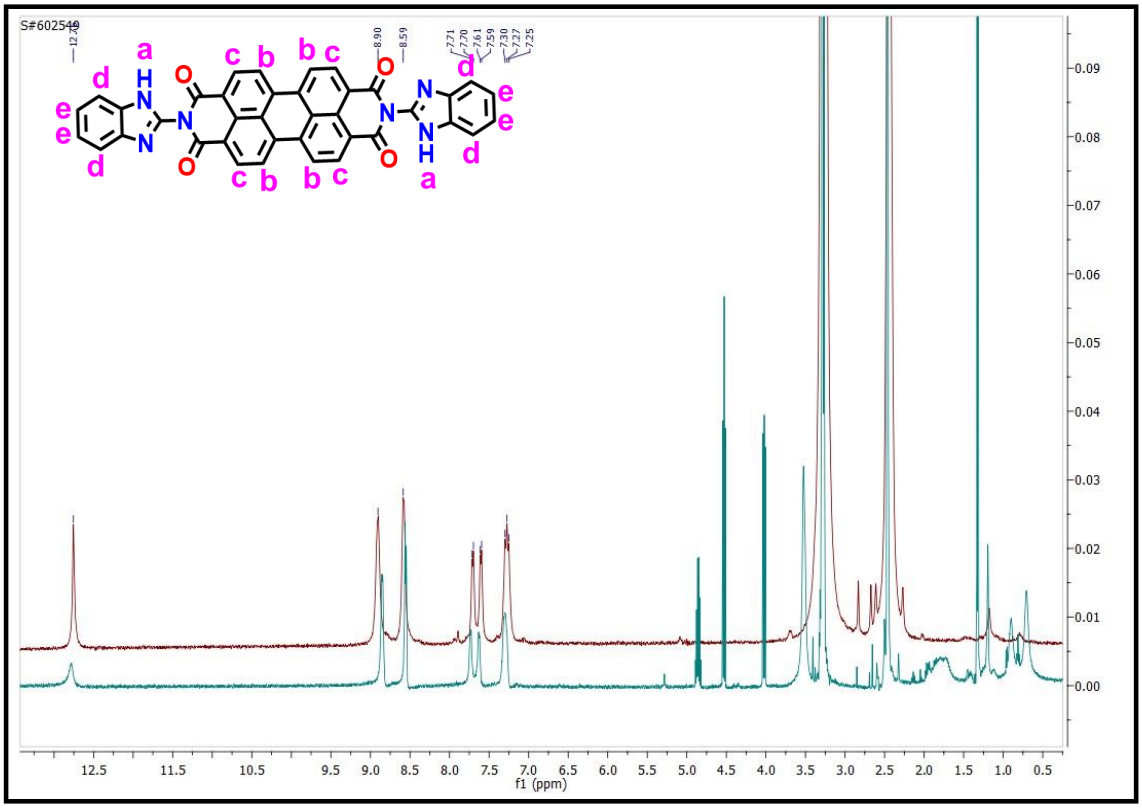

Figure S18: Comparison of ^{1}H NMR spectrum of PDI-AB molecule before (red) and after (green) GCD cycles (DMSO-d_6).

16. Mass spectrum of PDI-AB after 2000th GCD cycles:

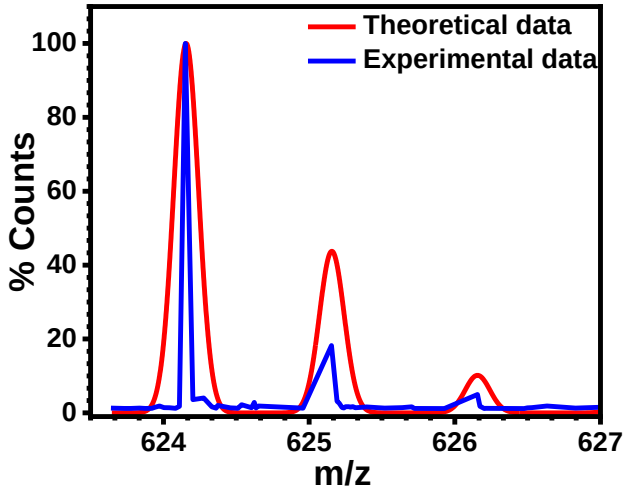

Figure S19: HRMS (ESI-MS positive mode) of PDI-AB mass spectra after 2000th GCD cycles.

17. X-ray photoelectron spectra analysis of PDI-AB after 2000th GCD cycles:

X-ray photoelectron spectroscopy measurements were performed on a device after 2000 GCD cycles, which contains PDI-AB, Nafion, and PMMA-$LiClO_4$-PC. Our primary objective was to identify and assign the PDI-AB-related peaks within the spectra.

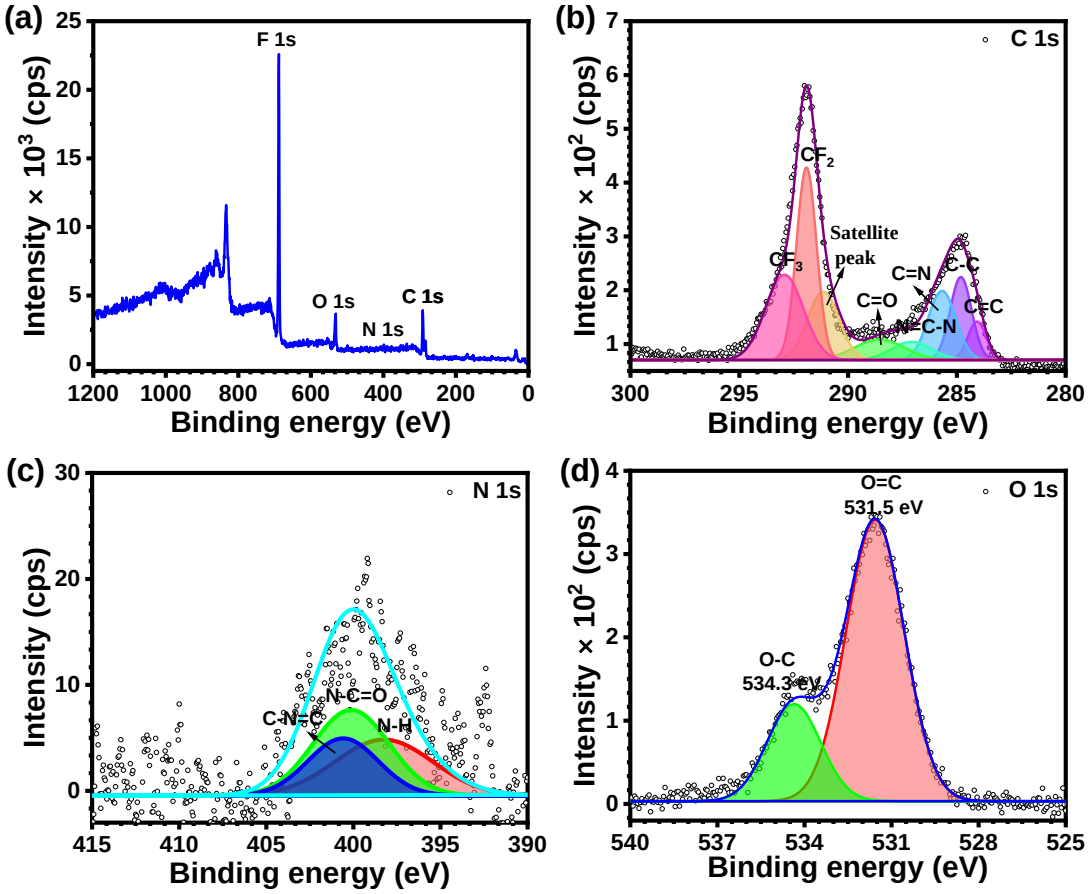

Figure S20: X-ray photoelectron spectroscopy measurements results after 2000th cycles. (a) Full survey scan of PDI-AB/ITO confirming the presence of C 1s, N 1s, and O 1s, (b) XPS spectra of C 1s orbital, (c) XPS spectra of N 1s orbital, and (d) XPS spectra of O 1s.

18. FE-SEM images of PDI-AB before and after 2000th GCD cycles:

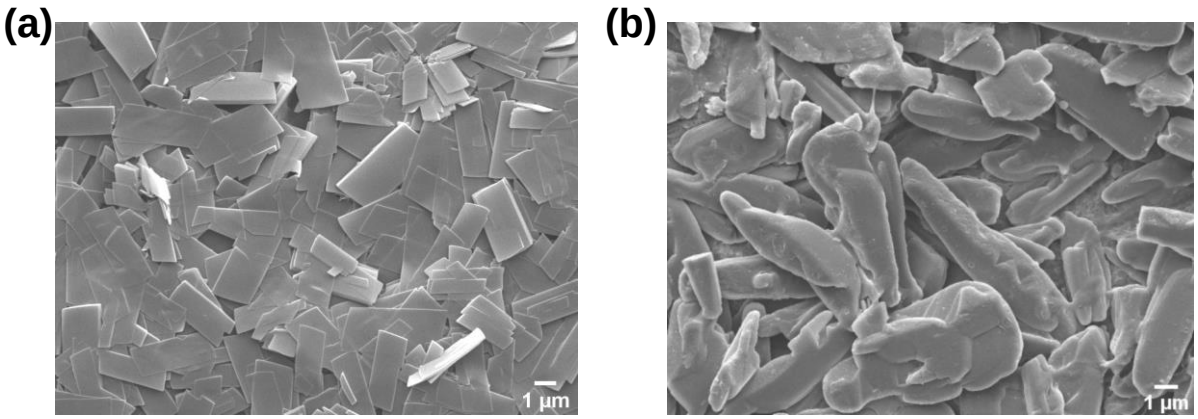

Figure S21: FESEM image of PDI-AB/ITO (a) Before GCD cycles, and (b) After 2000th GCD cycles at a 1.5 mA/g current density.

19. Log j vs. Log ν (b-value) plots: The plot of log j vs log ν for different voltage ranges from +0.25 V – (+1.25) V. The b-values are obtained through linear fitting and the b-values are in the range of 0.99 – 0.66 which lies in between the SCs and the batteries, suggesting the coexistence of diffusive and capacitive charge storage mechanism at the electrode/electrolyte interface and confirms the capacitive and diffusive nature of the supercapattery.[2,3]

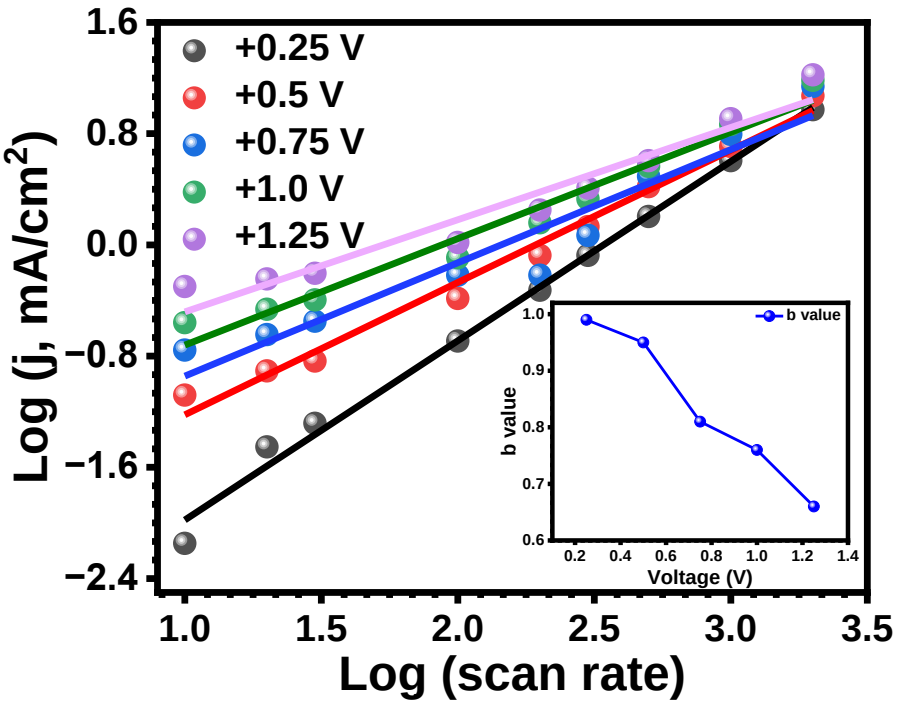

Figure S22: Log j vs. Log ν (b-value) plots at different voltages.

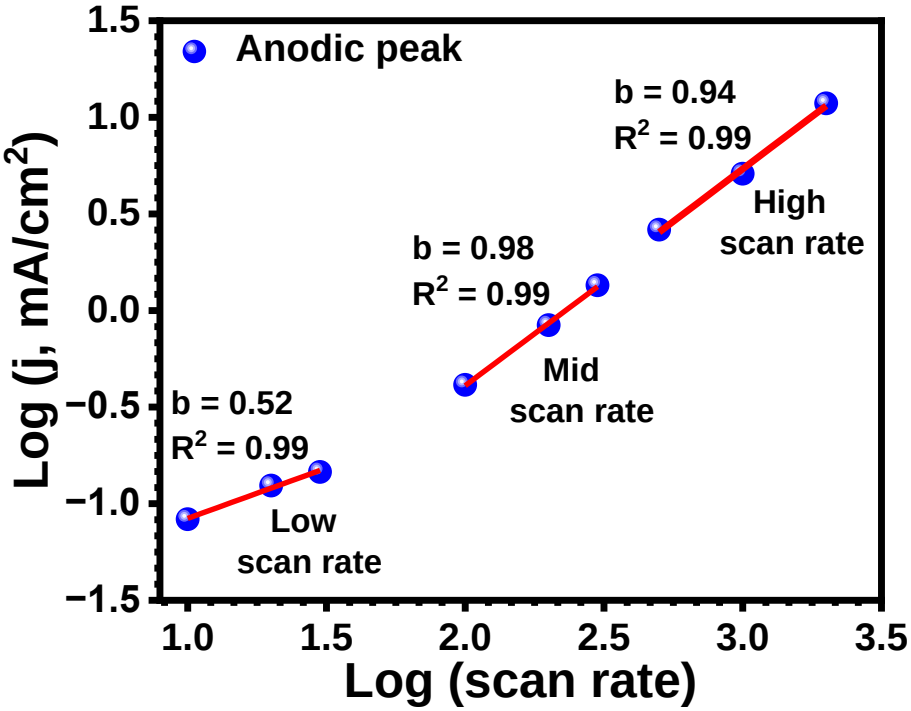

Figure S23: Log j vs. Log ν (b-value) plots at different +0.5 V voltage.

20. j (V).$\nu^{-1/2}$ vs. $\nu^{1/2}$ plot:

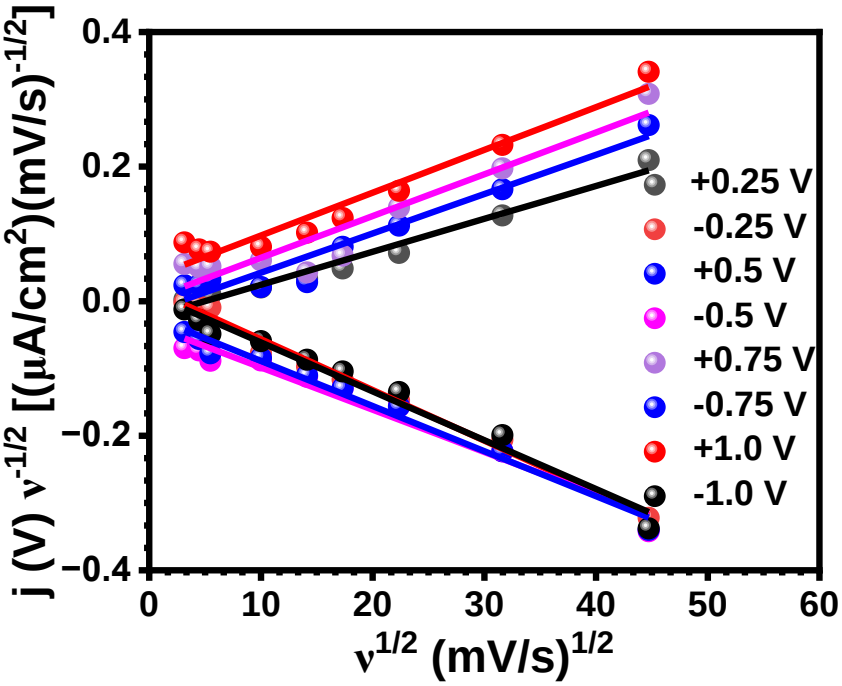

Figure S24: Linear fitting of the k_1 and k_2 parameters in the sweep rate range of 10–2000 mV s^{-1} (R^2 value lies between 0.94 to 0.98).

21. Electrochemical Impedance Spectra for SSC device:

Table S3. EIS fitted parameters for rigid ITO/PDI-AB//PMMA-LiClO$_4$-PC//PDI-AB/ITO SSC device.

Parameters	R_{CT} (Ω)	R_{MJ} (KΩ)	C_{MJ} (μF)	Z_W	CPE
PDI-AB	33.4±8.8	4.4±2.5	10.4±1.2	3.4±2.9	$Y_0=14.08\times10^{-6}$, N=0.91

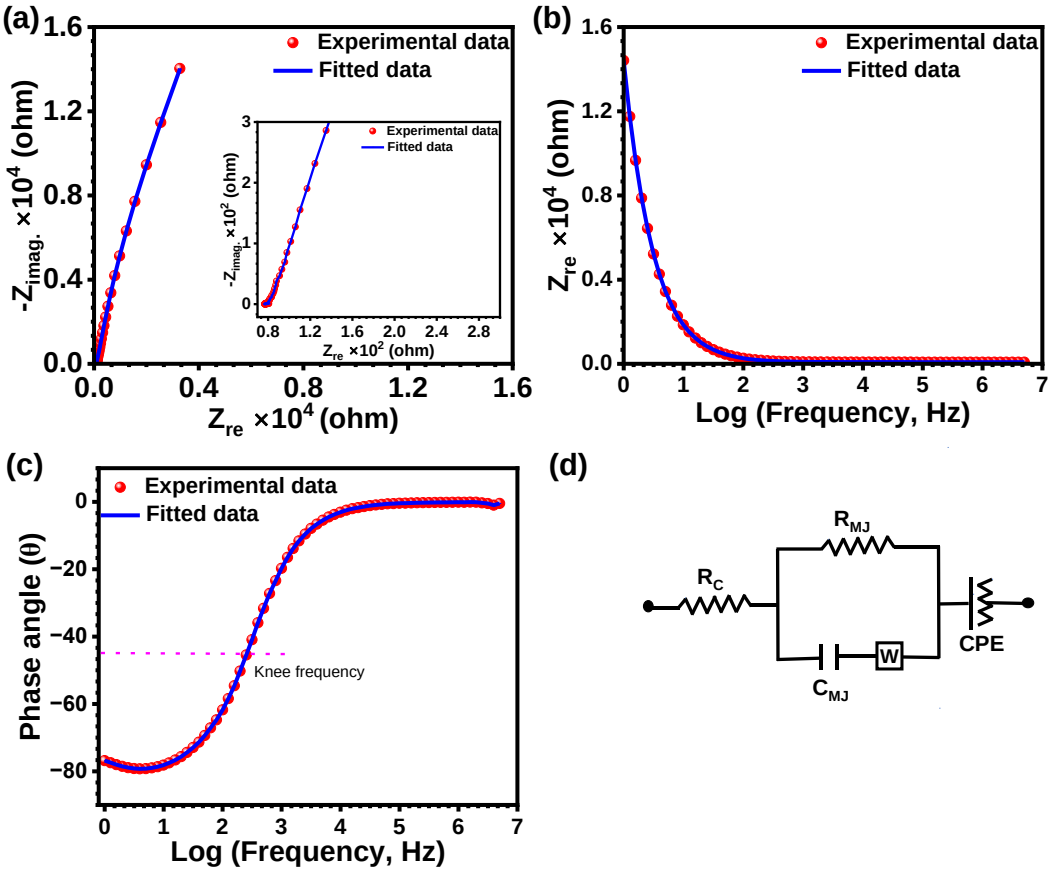

Figure S25: (a) Nyquist plot (experimental and fitted data), Bode plots, (b) |Z| vs frequency, (c) phase angle vs frequency, and (d) The Randles equivalent fitted circuit model of the rigid ITO/PDI-AB//PMMA-$LiClO_4$-PC//PDI-AB/ITO SSC device.

22. Cyclic stability and different bend angles measurement:

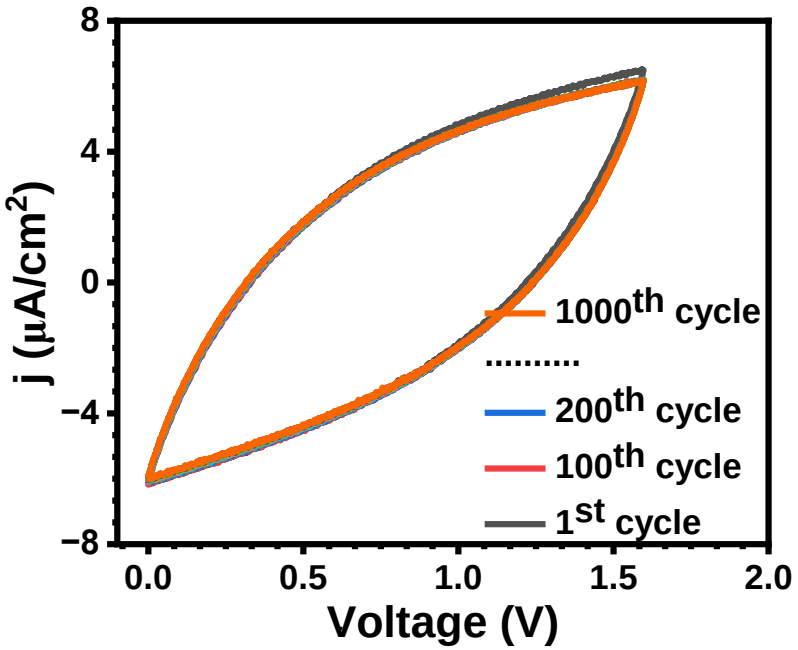

Figure S26: JV hysteresis loop of ITO/PDI-AB//PMMA-$LiClO_4$-PC//PDI-AB/ITO device with flexible ITO, potential range 0 to +1.6 V at 1000 mV/s scan rates up to 1000 cycles.

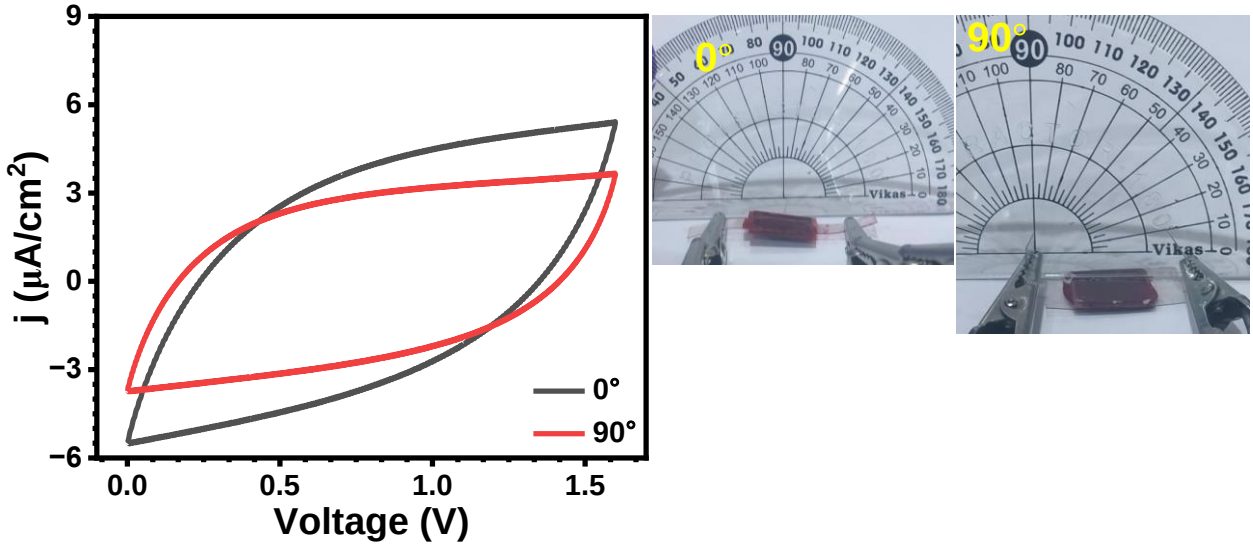

Figure S27: JV hysteresis loop of ITO/PDI-AB//PMMA-$LiClO_4$-PC//PDI-AB/ITO device with flexible ITO at different bend angles, potential range 0 to +1.6 V at 1000 mV/s scan rates.

Table S4: Capacitance comparison of PDI-AB with previous reports.

S. No.	Materials	Capacitance	References
1.	P(PDI-alt-BDT)	35 (mF/g)	[4]
2.	Naphthalene diimide pyridine/GF*	132 (F/g)	[5]
3.	Perylene diimide-pyridine/GF*	197 (F/g)	[5]
4.	P(NDI2OD-T2 vinylene linked (P2)	40 (F/g)	[6]
5.	PTCDA	63 mF/g	[7]
6.	benzoic-PDI	98.4 mF/g	[8]
7.	PDI-AB rigid device PDI-AB flexible device	33.87±0.66 (mF/g) 32.68±0.44 (mF/g)	This work

* GF = Graphite foil

23. Electrochemical parameters for equivalent circuit model:

Table S5. EIS fitted parameters for flexible ITO/PDI-AB//PMMA-$LiClO_4$-PC//PDI-AB/ITO SSC device

Angle	R_{CT} ($K\Omega$)	R_{MJ} (Ω)	C_{dl} (nF)	W	CPE
0°	*1.59±9.8*	*234.1±22.9*	180.8±*33.05*	*245*±52.8 ×10^{-6}	Y_0=11.51×10^{-6}, N=0.97
90°	*1.59±9.7*	*227.1±22.9*	184.9±*34.63*	*235.5*±47.78 ×10^{-6}	Y_0=12. 18×10^{-6}, N=0.97

24. Photocurrent measurements:

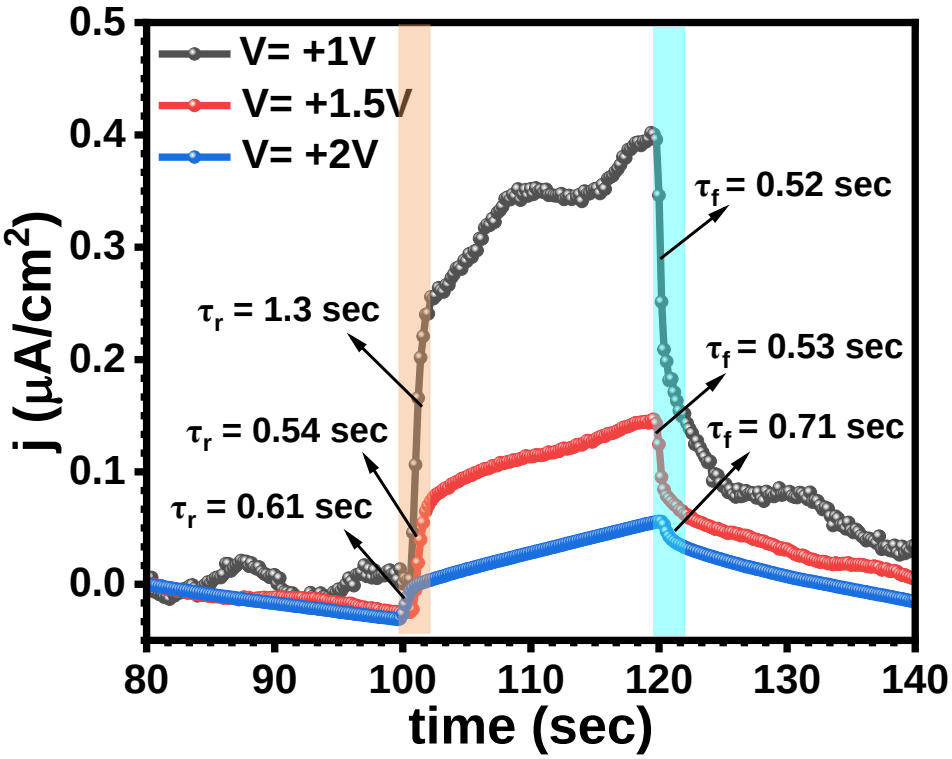

Figure S28: Comparison photocurrent measurement of ITO/PDI-AB//PMMA-$LiClO_4$-PC//PDI-AB/ITO at three different voltages (+1, +1.5, +2V).

Table S6: Comparative Table for photocurrent response of PDI-AB.

S. No.	Materials	Responsivity (mA/W)	References
1.	Pyrenodiindole (PDI)	0.1	[9]
2.	Pyrenodi (PDAI)	0.1	[9]
3.	Perylene/GO	110	[10]
4.	ITO/PDI-AB//PMMA-$LiClO_4$-PC//PDI-AB/ITO	0.8×10^{-3}	This work

* GO = Graphene Oxide

25. References:

1 S. Kim, C. Lee, S. Lee, S. H. Baek, D.-H. Ko and W.-S. Han, *J. Mater. Res. Technol.*, 2022, **17**, 2675–2683.

2 M. Z. Iqbal, M. M. Faisal, M. Sulman, S. R. Ali, A. M. Afzal, M. A. Kamran and T. Alharbi, *J. Energy Storage*, 2020, **29**, 101324.

3 A. Cymann-Sachajdak, M. Graczyk-Zajac, G. Trykowski and M. Wilamowska-Zawłocka, *Electrochim. Acta*, 2021, **383**, 138356.

4 S. Sharma, R. Soni, S. Kurungot and S. K. Asha, *J. Phys. Chem. C*, 2019, **123**, 2084–2093.

5 M. R. Biradar, A. M. Kale, B. C. Kim, S. V. Bhosale and S. V. Bhosale, *Energy Technol.*, 2022, **10**, 1–10.

6 S. Sharma, R. Soni, S. Kurungot and S. K. Asha, *Macromolecules*, 2018, **51**, 954–965.

7 D. Tian, H.-Z. Zhang, D.-S. Zhang, Z. Chang, J. Han, X.-P. Gao and X.-H. Bu, *RSC Adv.*, 2014, **4**, 7506.

8 M. E. Bhosale and K. Krishnamoorthy, *Chem. Mater.*, 2015, **27**, 2121–2126.

9 P. Gómez, J. Wang, M. Más-Montoya, D. Bautista, C. H. L. Weijtens, D. Curiel and R. A. J. Janssen, *Sol. RRL*, 2021, **5**, 1–11.

10 H.-S. Zhang, X.-M. Dong, Z.-C. Zhang, Z.-P. Zhang, C.-Y. Ban, Z. Zhou, C. Song, S.-Q. Yan, Q. Xin, J.-Q. Liu, Y.-X. Li and W. Huang, *Nat. Commun.*, 2022, **13**, 4996.